Charge-density wave transition of $1T$-VSe_2 studied by angle-resolved photoemission spectroscopy

K. Terashima, T. Sato, H. Komatsu, and T. Takahashi
Department of Physics, Tohoku University, Sendai 980-8578, Japan

N. Maeda and K. Hayashi
Okayama University of Science, 1-1 Ridai-cho, Okayama 700-0005, Japan

(Received 2 June 2003; published 13 October 2003)

High-resolution angle-resolved photoemission spectroscopy (ARPES) has been performed on a layered transition-metal dichalcogenide (TMDC) $1T$-VSe_2 to study the (4×4) charge-density wave (CDW) mechanism. We observed a partial Fermi-surface (FS) nesting on the electronlike FS centered at the M (L) point. The spectral weight near E_F is considerably suppressed below the transition temperature ($T_c=110$ K) around the nested portion, while a negligible spectral change is observed even across T_c in other portions of FS. This suggests that the CDW transition in $1T$-VSe_2 is caused by the three-dimensional FS nesting. Implications are discussed in relation to the physical properties of $1T$-VSe_2 as well as the ARPES results of other TMDC's.

DOI: 10.1103/PhysRevB.68.155108 PACS number(s): 71.18.+y, 71.30.+h, 71.45.Lr, 79.60.−i

I. INTRODUCTION

Layered transition-metal dichalcogenides (TMDC's) have attracted much attention because they show a variety of charge-density-wave (CDW) behaviors. In particular, $1T$-VSe_2 has attracted considerable interest. It exhibits a (4×4) CDW transition below $T_c=110$ K (Ref. 1) and the transport and magnetic properties show peculiar and characteristic anomalies at T_c (Ref. 2). $1T$-VSe_2 has a $1T$-CdI_2-type crystal structure [D_{3d} (Ref. 3) space group], where V atoms form a hexagonal sheet sandwiched by Se atoms [Fig. 1(a)]. These Se-V-Se sandwiches are stacked without lateral displacement and are coupled to each other by a weak van der Waals interaction. The overall crystal symmetry is threefold (trigonal) with inequivalent ΓM and $\Gamma M'$ directions in the Brillouin zone [Fig. 1(b)]. X-ray and electron-diffraction experiments revealed the satellite reflection due to the periodic lattice distortion (PLD),[1,3] whose wave vector has a large component normal to the layer despite the two-dimensional nature of the crystal. It has also been found that the PLD wave vector is commensurate within the layer, but is incommensurate perpendicular to it.[1] These behaviors have been theoretically investigated in terms of the wiggling of the Fermi surface (FS) perpendicular to the layer.[4]

To understand the mechanism of the CDW in $1T$-VSe_2, the electronic structure has been intensively studied by various experimental techniques.[3,5–16] Using angle-resolved photoemission spectroscopy (ARPES), Hughes *et al.*[5] determined the overall valence-band structure, which consists of a half-filled V $3d$ band near the Fermi level (E_F) and several dispersive Se $4p$ bands in the high-binding energy region. They discussed the observed reduction of the d-band intensity along the ΓM (AL) direction in terms of the incipient CDW instability. A subsequent ARPES study by Johnson *et al.*[8] suggested that there is a direct overlap between the p and d bands at the Γ (A) point near E_F, producing a small hole pocket at the center of the Brillouin zone. The band dispersions along the c^* axis (ΓA direction) were determined by photon-energy-dependent ARPES (Refs. 10–12) and the unoccupied band structure was investigated by angle-resolved inverse photoemission spectroscopy[6,7] (ARIPES) and very low-energy electron diffraction (VLEED).[12] In spite of these intensive studies on the electronic structure, the mechanism of the CDW transition in $1T$-VSe_2 has not been elucidated, because the energy scale and the CDW amplitude are much smaller than those of other $1T$-TMDC's.[13,14] The difficulty in growing a high-quality single crystal[17] may also have limited the elucidation.

In this paper, we report a high-resolution ARPES study on a high-quality $1T$-VSe_2 single crystal. By using the ultrahigh energy resolution (<10 meV) in ARPES measurements, we have succeeded in directly observing the CDW gap and the momentum dependence of gap amplitude on the FS. We compare the present experimental results with those for other $1T$-TMDC's (Refs. 18–21) and discuss the mechanism of the CDW transition of $1T$-VSe_2.

II. EXPERIMENTS

Single crystals of $1T$-VSe_2 were grown by the chemical vapor transport method. The starting materials were 99.5% vanadium powder and selenium shot. Crystals were grown in an evacuated sealed quartz tube with excess-selenium vapor transport at 700 °C for 7 days after being preheated at 850 °C for 3 days. The obtained crystals are platelet and as large as $5\times5\times0.1$ mm^3. The thermogravimetric analysis

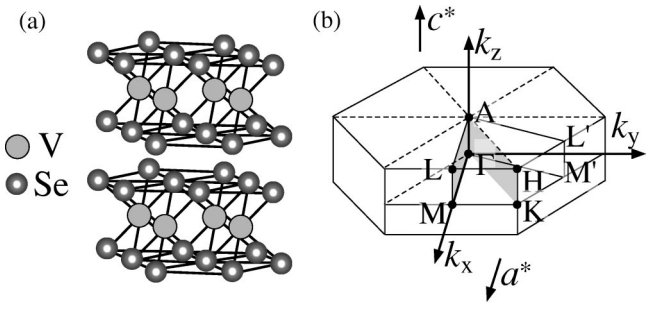

FIG. 1. (a) Crystal structure and (b) Brillouin zone of $1T$-VSe_2.

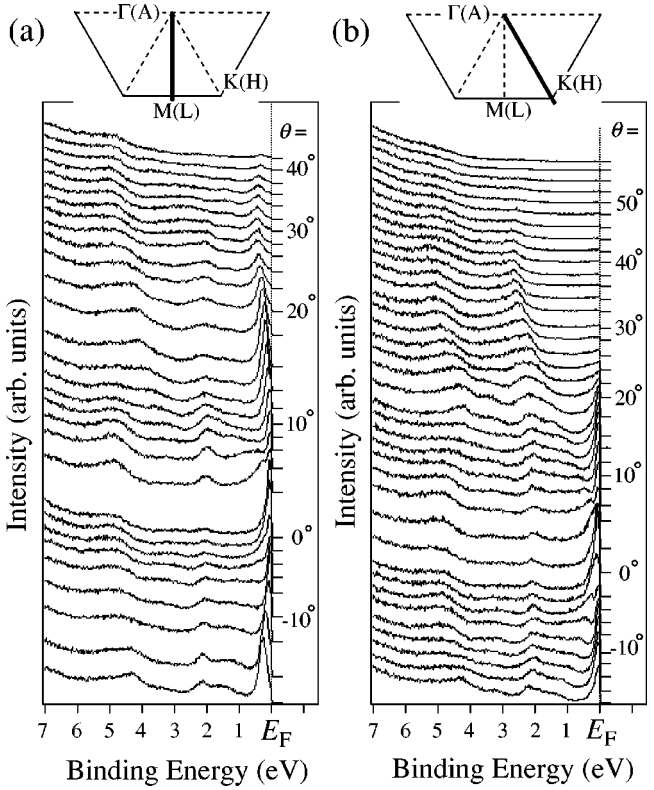

FIG. 2. Valence-band ARPES spectra of $1T$-VSe_2 measured at 30 K with He Iα resonance line along (a) ΓM (*AL*) and (b) ΓK (*AH*) directions. Polar angle (θ) referred to the surface normal is denoted on spectra.

shows that the crystals are stoichiometric within 1% experimental accuracy.[17]

ARPES measurements were performed using a GAMMADATA-SCIENTA SES-200 spectrometer with a high-flux discharge lamp and a toroidal grating monochromator. He Iα ($h\nu = 21.218$ eV) and He IIα ($h\nu = 40.814$ eV) resonance lines were used to excite photoelectrons. The energy and angular (momentum) resolutions were set at 9–17 meV and 0.3° (0.01 $Å^{-1}$), respectively. A clean surface for ARPES measurements was obtained by *in situ* cleaving of crystal in an ultrahigh vacuum of 3×10^{-11} Torr. The Fermi level (E_F) of the sample was referenced to that of a gold film evaporated onto the sample substrate.

III. RESULTS AND DISCUSSION

A. Valence-band region

Figure 2 shows valence-band ARPES spectra of $1T$-VSe_2 measured at 30 K along the ΓM (*AL*) and ΓK (*AH*) directions in the Brillouin zone. We find a very sharp peak near E_F in the spectra for both directions, which is ascribed to the V $3d_{z^2}$ band.[5,8,10–12] Several other peaks located at 1–6 eV are assigned to the Se $4p$ bands. The overall dispersive feature of peaks appears to be similar in both directions at around $\theta = 0°$, while the difference becomes remarkable in the large polar-angle region of $\theta = 20°$–$40°$. For example,

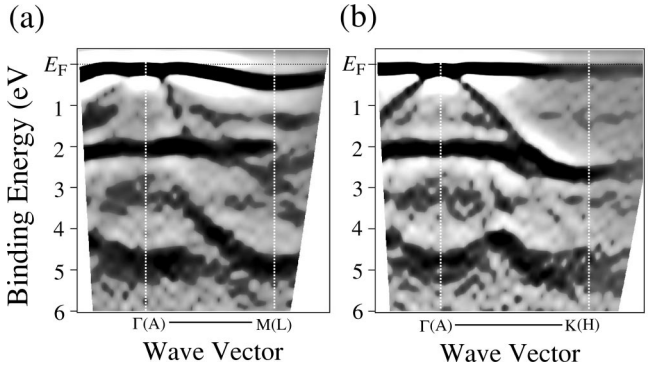

FIG. 3. Experimental band structure of $1T$-VSe_2 along (a) ΓM (*AL*) and (b) ΓK (*AH*) directions.

the V $3d_{z^2}$ band is clearly seen below E_F even at $\theta = 30°$–$40°$ in the ΓM (*AL*) direction, while it disappears at around $\theta = 20°$ in the ΓK (*AH*) direction. The Se $4p$ band at 2 eV shows a very weak dispersion along the ΓM (*AL*) direction, although it shows a sizable dispersion along the ΓK (*AH*) direction. Thus the measured ARPES spectra clearly represent the characteristic band structure for two different directions in the Brillouin zone. It is noted that the present ARPES result with respect to the gross feature of the valence band is consistent with previous ARPES results,[5,8,10–12] while the characteristic structures are better resolved in the present ARPES spectra.

To see more clearly the dispersive feature of bands in the ARPES spectra, we have mapped out the ''band structure'' and show the result in Fig. 3. The experimental band structure has been obtained by taking the second derivative of ARPES spectra and plotting the intensity on a square-root scale by gradual shading as a function of the wave vector and binding energy.[22] Dark areas correspond to the experimental bands. It is noted that all of the previous ARPES studies on $1T$-VSe_2 mapped the band structure by determining the peak positions in ARPES spectra by eyes/hand. To avoid an artificial error and/or a background effect due to secondary electrons, we employed the above numerical method. As seen in Fig. 3, we observe several dispersive features in both directions. A weakly dispersive band near E_F is ascribed to the V $3d_{z^2}$ band, while the others are assigned to the Se $4p$ σ bands. The almost nondispersive band at 2 eV is assigned to the Se $4p_{x,y}$ band,[12] while a band located near E_F at the Γ (*A*) point having a remarkable downward dispersion toward the zone boundary is ascribed to the Se $4p_z$ band.[12]

We show in Fig. 4 the comparison of the experimental band structure with three different band calculations; the linear augmented plane-wave (LAPW) calculation by Brauer *et al.*[11] [Figs. 4(a) and 4(b)], the first-principles self-consistent non-muffin-tin calculation by Zunger and Freeman[23] [Figs. 4(c) and 4(d)], and the layer-method calculation by Woolley and Wexler[4] [Figs. 4(e) and 4(f)]. We find in Fig. 4 that the gross dispersive features of bands appear to be similar for the three band calculations, and show a qualitative agreement with the experimental results. However, there are several quantitative disagreements between each calculation and the experiment.

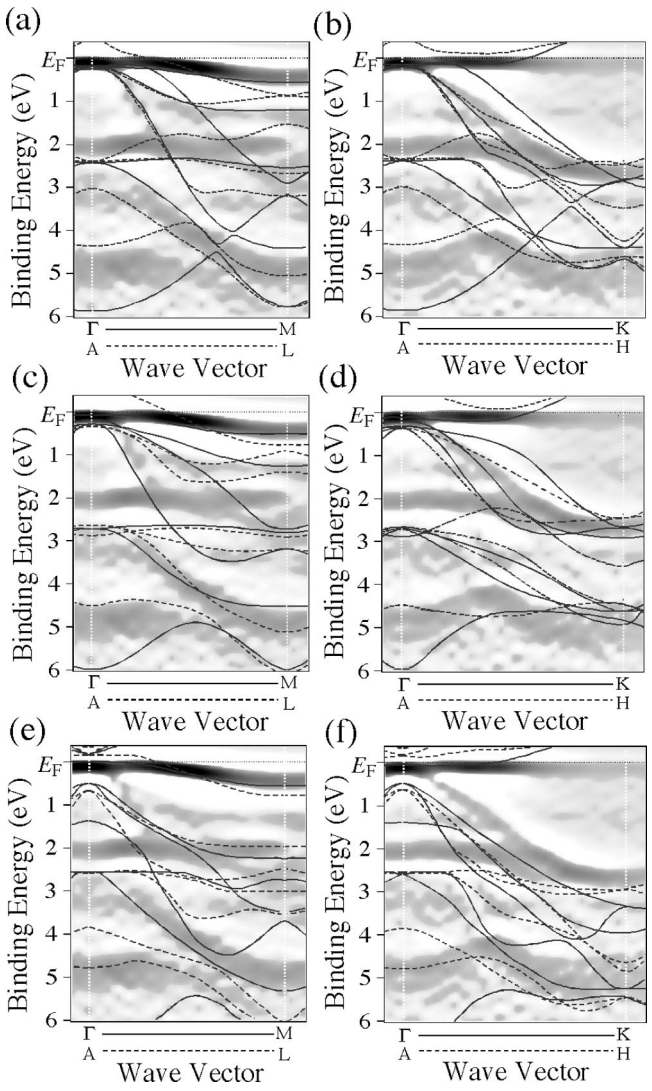

FIG. 4. Comparison of the experimental valence-band structure with the band calculations; (a) and (b) for the LAPW band calculation (Ref. 11), (c) and (d) for the first-principles self-consistent band calculation (Ref. 23), and (e) and (f) for the layer-method band calculation (Ref. 4). Thin solid and broken lines show the calculated bands.

For example, both the LAPW and the first-principles calculations trace the experimental bands relatively well, while the layer-method calculation appears to deviate from the experimental result. The deviation is most prominent in the energy position of the Se $4p$ band. The top of the Se $4p$ band at the Γ (A) point is shifted toward a higher binding energy by 0.5 eV in the layer-method calculation in comparison with the experiment. It is also found that the flat band located at 2 eV in the experiment is well reproduced by the LAPW calculation, while the same band in the other calculations is clearly shifted toward a higher binding energy. All of these findings indicate that the LAPW band calculation serves as a good theoretical basis for understanding the gross valence-band structure of $1T$-VSe_2.

B. Near-E_F region

Figure 5 shows high-resolution ARPES spectra near E_F measured at 30 K along the ΓM (AL) and ΓK (AH) directions. We find in Fig. 5(a) that two bands disperse near E_F in the ΓM (AL) direction. The first band has the top of its dispersion immediately below E_F at the Γ (A) point and steeply disperses toward the high binding energy on going to the M (L) point. The second one appears at E_F, midway between the Γ (A) and M (L) points, and shows a relatively slow dispersion toward the zone boundary. The first band is assigned to the Se $4p_z$ band, while the second one is attributed to the V $3d_{z^2}$ band. It is clear from Fig. 5(a) that the experimental V $3d_{z^2}$ band crosses E_F at a point around $\theta = 6$-$10°$. There is a clear difference between the two directions in terms of the band dispersion near E_F. The V $3d_{z^2}$ band monotonically disperses toward the high binding energy on increasing the polar angle from $\theta = 6$-$10°$ in the ΓM (AL) direction, while the same band again enters into the unoccupied states at around $\theta = 20°$ in the ΓK (AH) direction. The V $3d_{z^2}$ band in the ΓK (AH) direction shows a very flat dispersion with the maximum intensity at around $\theta = 15°$, suggesting that the band has a bottom around this point.

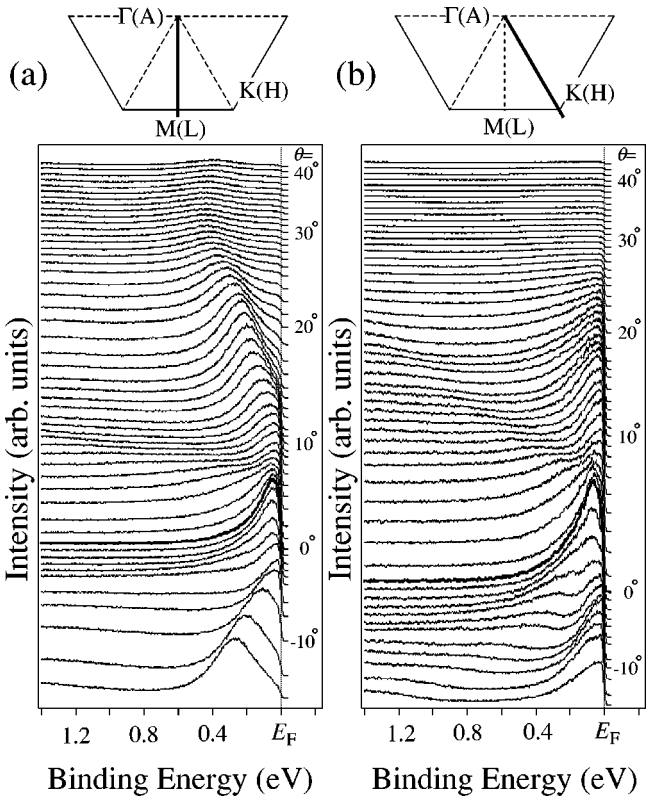

FIG. 5. ARPES spectra in the vicinity of E_F of $1T$-VSe_2 measured at 30 K with a He Iα resonance line along (a) ΓM (AL) and (b) ΓK (AH) directions.

Figure 6 shows the comparison of the experimental band dispersion near E_F with the three calculations. We find that the experimental band dispersion is qualitatively well reproduced by each calculation, for example, the dispersive feature of the V $3d_{z^2}$ band along the ΓM (AL) direction. However, a closer look reveals quantitative disagreements between the experiment and the calculations. As shown in

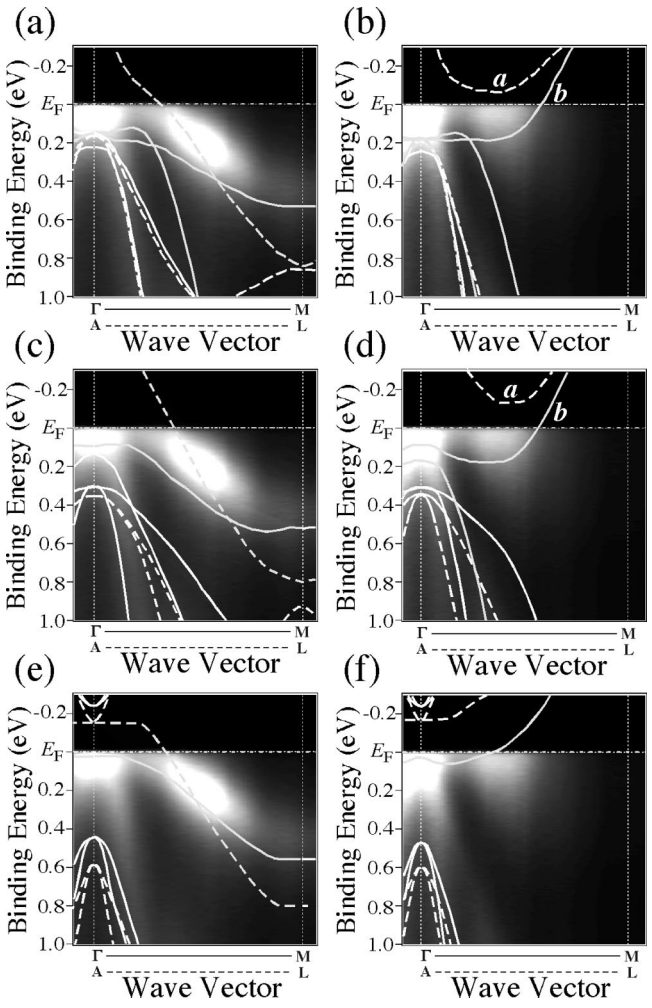

FIG. 6. Experimental band structure near E_F (bright areas) obtained by plotting the ARPES intensity as a function of binding energy and momentum, compared with three band structure calculations: (a) and (b) for the LAPW band calculation (Ref. 11), (c) and (d) for the first-principles self-consistent band calculation (Ref. 23), and (e) and (f) for the layer-method band calculation (Ref. 4). Thin solid and broken lines show the calculated bands.

Figs. 6(e) and (f), the layer-method calculation has predicted that the top of the Se $4p$ band is located at 0.5 eV, although the experimental Se $4p$ band has the top of the dispersion immediately below E_F (less than 0.1 eV from E_F). It is noted here that the strong intensity around the Γ (*A*) point in the experiment is reminiscent of a small electron pocket centered at the Γ (*A*) point. However, this is not the case because (i) the corresponding band is not seen in the calculations, and (ii) we do not observe two intensity maxima at E_F at both sides of the Γ (*A*) point indicative of band crossing. It is also found in Fig. 6 that the energy position of the V $3d_{z^2}$ band at the M (L) point is much closer to E_F in the experiment (0.5 eV from E_F) than in the calculations (0.6-0.8 eV from E_F). The E_F-crossing point of the V $3d_{z^2}$ band (namely, the Fermi vector k_F) along the Γ*M* (*AL*) direction in the experiment shows a good agreement with k_F in the AL direction in the calculations.

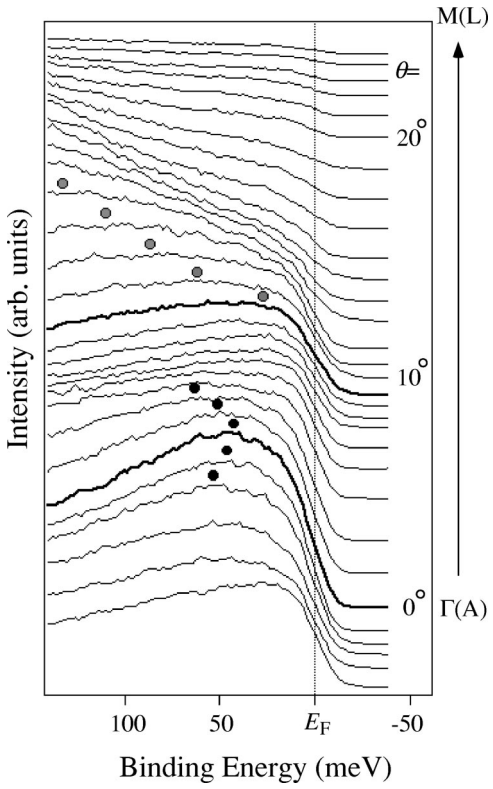

FIG. 7. ARPES spectra of $1T$-VSe_2 in the vicinity of E_F measured at 30 K along Γ*M* (*AL*) direction. Filled circles show the peak positions of spectra.

In contrast with the Γ*M* (*AL*) direction, the situation in the Γ*K* (*AH*) direction seems complicated. We find a finite intensity at E_F between the Γ (*A*) and *K* (*H*) points in the experiment. The band at E_F does not show any dispersion, but only loses its weight on approaching both the Γ (*A*) and *K* (*H*) points. A corresponding band which gives this characteristic intensity variation is not seen in the layer-method calculation [Fig. 6(f)], while a band with similar characteristics is found in the unoccupied states of the LAPW [Fig. 6(b)] and the first-principles [Fig. 6(d)] calculations (band *a*). Since the temperature of the measurement is sufficiently low (30 K), the finite intensity at E_F observed in the experiment is not explained by the thermally broadened tail of band *a* in the unoccupied states. Taking into account of the fact that bands *a* and *b* in Fig. 6 are originally the same band dispersing along the k_z direction, it is most probable that the finite intensity at E_F can be ascribed to the intermediate portion of the band between the Γ*K* and *AH* high-symmetry lines.

One of the important questions concerning the experimental band structure of $1T$-VSe_2 is whether the Se $4p$ band crosses E_F and gives rise to a small hole pocket centered at the Γ (*A*) point. This is crucial in clarifying whether holes in the *p* band play an important role for the CDW in $1T$-VSe_2. We show the ARPES spectra in the vicinity of E_F measured along the Γ*M* (*AL*) direction in Fig. 7. As is clearly seen in Fig. 7, the peak at $\theta=0°$ [namely, at the Γ (*A*) point] is located 40–50 meV away from E_F. This indicates that the band does not reach E_F since the Fermi-edge cutoff indica-

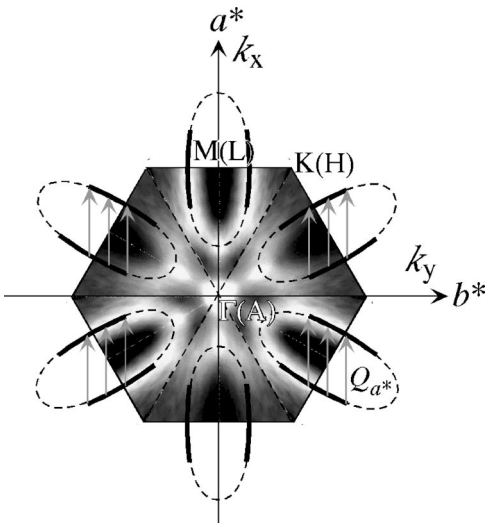

FIG. 8. Fermi surface of 1T-VSe_2 obtained by plotting the ARPES intensity at E_F as a function of two-dimensional momentum. The ARPES intensity is estimated by integrating the spectral weight within 20 meV with respect to E_F, and symmetrized by assuming the trigonal symmetry. Bright areas show the strong intensity and dashed lines trace the local maxima of the intensity, showing a rough sketch of the Fermi surface. Thick solid lines indicate the straight portion of the Fermi surface. Gray arrows show the nesting vector determined by the present ARPES experiment.

tive of the E_F crossing is expected to appear within 10 meV of E_F. In contrast, the V $3d_{z^2}$ band located at around 120 meV at $\theta=13°$ shows a steep dispersion toward E_F on decreasing the polar angle and appears to reach E_F at $\theta=9°$. On further decreasing the polar angle, the intensity of the peak suddenly decreases. This indicates that the band crosses E_F at around $\theta=9°$. Thus, the present experimental results clearly show that there is no FS due to the p band at the $\Gamma(A)$ point, contrary to the suggestion from the previous ARPES work.[8] However, the thermal excitation of electrons at the top of the p band to the conduction band (unoccupied states) is likely to occur at high temperatures since the energy position (40 meV from E_F) is well within the thermal broadening of the Fermi-Dirac (FD) function at high temperatures (for example, $3k_BT$ at 300 K is 100 meV). Since the velocity of the p band near E_F is much larger than that of the d band as seen in Fig. 5(a), the holes with higher mobility may contribute substantially to the electric conductivity at high temperatures. This is consistent with the experimental finding that the Hall coefficient has a positive sign at temperatures higher than 310 K.[24,25]

It is noted here that no discernible variations in the overall dispersion are observed even across T_c (up to 180 K), showing that band folding caused by the (4×4) reconstruction is considerably weak, probably due to the small Fourier component of the CDW potential[18,19,26] and/or the small size of the reconstructed Brillouin zone.[19]

C. Fermi surface topology

In Fig. 8, we show the ARPES-intensity plot at E_F of 1T-VSe_2 as a function of the two-dimensional wave vector, measured with the He IIα resonance line at 30 K. The intensity is obtained by integrating the spectral weight within 20 meV with respect to E_F and is symmetrized on the assumption of the trigonal symmetry. We also show the position of the FS by broken lines obtained by tracing the local maximum of the intensity. In Fig. 8, we observe two distinct features: one is a large ellipsoidal FS centered at the M (L) point and another is an intense feature at the Γ (A) point. The large ellipsoidal FS is attributed to the V $3d_{z^2}$ band, while the strong intensity at the Γ (A) point is due to the Se $4p$ band whose top is located very close to, but below E_F. We find that the V $3d$-derived FS has a straight portion as shown by the thick solid line in Fig. 8, suggesting a good nesting condition of the FS in this specific momentum region. Assuming that the in-plane nesting vector has a component only along the a^* axis as reported from the XRD measurement,[1] we have estimated the nesting vector from the present ARPES experiment at $0.27\pm0.03a^*$. We have also performed photoemission measurements with another photon energy (He Iα; 21.218 eV), and obtained a similar value of $0.26\pm0.02a^*$ for the nesting vector. These values show a good agreement with the value obtained from the XRD experiment ($0.25a^*$).[1] It is thus found that electrons on this nested portion play an essential role in the formation of CDW in 1T-VSe_2. The volume of the electron pocket is estimated at $44\pm3\%$ of the whole Brillouin zone, confirming the half-filling nature of the d band.

Next we compare the topology of the FS between the experiment and the calculation. Band calculations[4,11,23] have predicted that there is an ellipsoidal electronlike FS centered at the A point in the ALH plane [see Fig. 1(b)] while the FS extends over the Γ point in the ΓKM plane, producing a FS with an open orbit. In the present ARPES experiment, the FS centered at the M (L) point does not reach the zone center and the overall shape is similar to that of the AHL plane in the calculation. This implies that the present ARPES observes the photoemission mainly from the AHL plane rather than the ΓKM plane. The small finite intensity at E_F along the ΓK (AH) line as seen in Fig. 8 may be due to the final-state broadening which gives an uncertainty in k_z in the photoemission process. As discussed in Fig. 6, the V $3d_{z^2}$ band crosses E_F at a specific k_z point between the ΓK and AH lines. Because of the final-state broadening, the electrons around this k_z are expected to contribute to the photoemission intensity measured in the ΓKHA plane.

To clarify the nature of the CDW gap at the nested portion of FS, we have performed detailed temperature- and momentum-dependent ARPES. In the next section, we report the direct observation of the CDW gap and discuss the mechanism of the CDW in 1T-VSe_2.

D. Charge-density-wave gap

Figure 9 shows ARPES spectra in the vicinity of E_F at various momenta (k) on the FS measured at two temperatures below and above T_c. At 30 K below T_c, the peak in the spectrum is located at about 20 meV in the k region near the Γ (A) point (spectra 1–5). On approaching the M (L) point on the FS, the peak gradually moves toward a higher binding

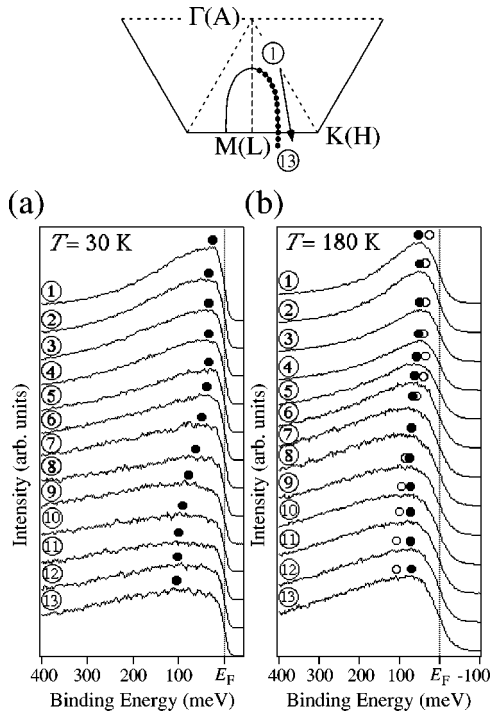

FIG. 9. ARPES spectra near E_F of $1T$-VSe_2 at (a) 30 K and (b) 180 K measured at several k_F points on the FS shown in the upper panel. The peak position in the spectra determined by fitting with Gaussian around the peak is indicated by filled circles. Peak positions of 30 K are shown by open circles in (b) for comparison.

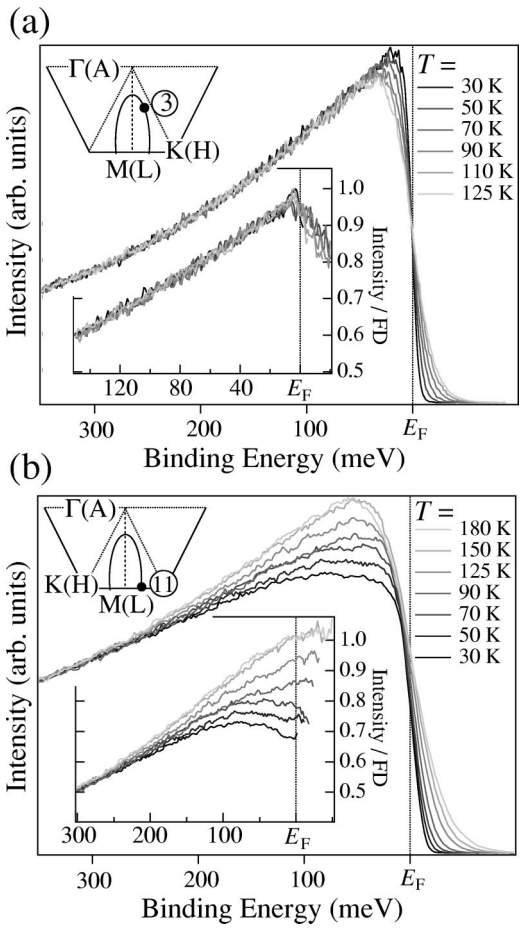

FIG. 10. Temperature dependence of ARPES spectra for $1T$-VSe_2 measured at two representative k_F points (points 3 and 11) in the Brillouin zone. Inset shows the partial DOS obtained by dividing ARPES spectra by the FD function at each temperature convoluted with the Gaussian resolution function. Spectral intensity is normalized by integrated spectral intensity from 0.7 to 1.4 eV.

energy and finally reaches 80–100 meV near the M (L) point (spectra 10–13). It is noted here that the k region where the peak is located at high energy (spectra 10–13) coincides well with the k region where the nesting condition is fulfilled as discussed above (see Fig. 8). This suggests that the observed anomalous k dependence of the peak position in the spectrum is closely related to the CDW formation in $1T$-VSe_2. In contrast to the strong k dependence of the ARPES lineshape below T_c, the k dependence of the spectrum above T_c is considerably weak as seen in Fig. 9(b), where the peak position at 180 K (filled circles) shows a much smaller k dependence and does not coincide with that below T_c (open circles). This obviously rules out the possibility of the band-structure effect for the anomalous k dependence of the peak position, and confirms that the distinct spectral difference across T_c is closely related to the CDW formation.

In order to clarify how the anomalous spectral feature evolves with temperature, we measured the temperature dependence of ARPES spectra at two representative k_F points. Results are shown in Fig. 10. The spectral intensity is normalized with the integrated intensity of 0.7–1.4 eV binding energy since it is expected that electrons at such high binding energy are not affected by the CDW formation. As shown in Fig. 10(a), the temperature dependence of the ARPES spectrum is symmetric with respect to E_F at point 3 where the nesting condition is found to be poorly fulfilled. The inset shows the partial density of states (DOS) obtained by dividing the ARPES spectra by the FD function at each temperature convoluted with the energy resolution. The partial DOS shows no or a negligible temperature dependence, indicating that electrons in this k region do not contribute to the CDW formation. In contrast, the temperature dependence at point 11 is anomalous as seen in Fig. 10(b), where we find a strong asymmetry of the spectral change with respect to E_F. Surprisingly, the peak at 50 meV systematically reduces its intensity on cooling, opposite to the behavior expected from the temperature dependence of the FD function. As a result, the spectral intensity at E_F is gradually depleted with decreasing temperature. Taking into account of the fact that the nesting condition is well fulfilled at point 11, we conclude that the observed spectral change reflects the opening of the CDW gap. It is remarked here that the Fermi edge is retained even below T_c. This suggests that the CDW gap is not a full gap but a pseudogap or a partial gap with a finite DOS at E_F. The pseudogap-opening behavior is more clearly illustrated in the inset, where the partial DOS near E_F, obtained by the same method as described above, shows a monotonic decrease with decreasing temperature, but has a finite weight at E_F even at 30 K far below T_c (110 K). It is also noted that the temperature-induced change of the DOS starts at about

150 K, which is much higher than T_c. All of these findings indicate that the gap opening starts at a temperature well above T_c and a finite DOS remains at E_F even below T_c. We speculate that the finite DOS at E_F below T_c is due to the three-dimensional nature of the nesting vector, as suggested by the XRD experiment[1] as well as the band calculation.[4]

Next we discuss the relationship between the pseudogap and the physical properties of $1T$-VSe_2. It has been reported that the electrical resistivity of $1T$-VSe_2 remains metallic even below T_c with a small bump structure at 70 K (Ref. 2). The metallic nature even below T_c is consistent with the existence of a pseudogap with a finite DOS at E_F below T_c, although we do not observe any anomalous behavior in the photoemission spectrum corresponding to the bump structure at 70 K in the electrical resistivity. It has been reported that the Hall coefficient changes its sign from positive to negative at around 310 K upon decreasing temperature, and shows a rapid decrease at around 120 K upon further lowering temperature.[2,24,25] The intrinsic magnetic susceptibility is temperature independent at high temperature, but gradually starts to decrease at around 150 K and then is steeply reduced at low temperatures below 120 K (Ref. 2). We consider that the reduction of DOS at E_F due to the formation of the pseudogap is responsible for the strong temperature dependence of both the Hall coefficient and the magnetic susceptibility. The slight decrease of the magnetic susceptibility above T_c may be related to the small variation of the DOS near E_F at temperatures between T_c and 150 K as shown in Fig. 10.

It is evident from Fig. 10(b) that the spectral weight in the nested region of the FS is depleted below T_c within 200 meV with respect to E_F. When we take the value 200 meV as the CDW-gap size Δ, $2\Delta/k_BT_c$ becomes 40, which is far larger than the mean-field value (3.52). The peak of the partial DOS is located at 80–100 meV binding energy at 30–50 K, as seen in the inset to Fig. 10(b). This value shows a good agreement with the peak position of the tunneling conductance spectrum at 60 K (80 meV).[14] This suggests that the size of the pseudogap is 80–100 meV and the $2\Delta/k_BT_c$ value is about 20, which is still much larger than the mean-field value. A similar substantial deviation of the CDW-gap value from the mean field theory has also been reported for other $1T$-TMDC's. For example, it has been reported that $1T$-$TaSe_2$ and $1T$-TaS_2 have $2\Delta/k_BT_c$ values of 12–35.[18,20,21] Thus, the relatively large $2\Delta/k_BT_c$ value seems a common feature for $1T$-TMDC's.

Finally, we compare $1T$-VSe_2 with $1T$-TaS_2, which is isostructural to $1T$-VSe_2 and has a FS similar to that of $1T$-VSe_2.[18,19] It is known that $1T$-TaS_2 shows a two-step CDW transition; the first one is a quasicommensurate (QC) CDW transition at 350 K and the second is a commensurate CDW transition at 180 K. It has been suggested that the QC-CDW of $1T$-TaS_2 is driven by the Mott localization[18,19] due to the strong electron correlation between d electrons. Previous ARPES studies on $1T$-TaS_2 (Refs. 18,19) have reported that a pseudogap opens all across the FS in the QC-CDW phase, and accordingly, no bands cross E_F anywhere in the Brillouin zone. In contrast, in $1T$-VSe_2, the pseudogap is observed only in a partial portion of the FS, and there is a band which crosses E_F even in the CDW phase. These remarkable differences in the pseudogap behavior suggest that the CDWs of these compounds have different origins. We conclude that the CDW of $1T$-VSe_2 is caused by the FS nesting, as is evident in the present ARPES study, while that of $1T$-TaS_2 in the QC-CDW phase may be induced by the Mott localization, as proposed previously.[18,19] This is supported by the experimental finding that the band structure of $1T$-VSe_2 determined by ARPES agrees well with the band structure calculation, suggesting that the electron correlation is less important in $1T$-VSe_2.

IV. SUMMARY

We performed high-resolution ARPES measurements on $1T$-VSe_2 to study the electronic band structure, the Fermi surface, and consequently the mechanism of CDW transition. We compared the experimentally determined band structure with three band calculations and found that the LAPW band calculation reproduces the experimental result well. We found an ellipsoidal electronlike Fermi surface centered at the M (L) point in the Brillouin zone, which has a relatively straight portion parallel to the a^* axis, which is indicative of a good nesting condition. The estimated nesting vector shows good agreement with that from the XRD experiment. We found that the partial density of states near E_F on the nested portion shows a remarkable suppression at low temperatures below T_c (110 K), but still has a substantial finite weight even at 30 K. This indicates that a pseudogap opens on the Fermi surface at low temperatures and the nesting vector has a substantial three-dimensional nature. We compared the present ARPES result with the physical properties of $1T$-VSe_2 and found a good correspondence. A comparison of ARPES results on $1T$-VSe_2 with those on $1T$-TaS_2 confirms that the CDW in $1T$-VSe_2 is caused by the three-dimensional Fermi-surface nesting, but not by the Mott localization.

ACKNOWLEDGMENTS

We thank Y. Iida and N. Takahashi for their help in the experiment. This work was supported by a grant from the MEXT of Japan.

[1] K. Tsutsumi, Phys. Rev. B **26**, 5756 (1982).
[2] A.H. Thompson and B.G. Silbernagel, Phys. Rev. B **19**, 3420 (1979).
[3] D.J. Eaglesham, R.L. Withers, and D.M. Bird, J. Phys. C **19**, 359 (1986).
[4] A.M. Woolley and G. Wexler, J. Phys. C **10**, 2601 (1977).
[5] H.P. Hughes, C. Webb, and P.M. Williams, J. Phys. C **13**, 1125 (1980).
[6] R. Claessen, I. Schäfer, and M. Skibowski, J. Phys.: Condens. Matter **2**, 10 045 (1990).

[7] A.R. Law, P.T. Andrews, and H.P. Hughes, J. Phys.: Condens. Matter **3**, 813 (1991).
[8] M.T. Johnson, H.I. Starnberg, and H.P. Hughes, J. Phys. C **19**, L451 (1986).
[9] H.I. Starnberg, P.O. Nilsson, and H.P. Hughes, J. Phys.: Condens. Matter **4**, 4075 (1992).
[10] H.I. Starnberg, H.E. Brauer, L.J. Holleboom, and H.P. Hughes, Phys. Rev. Lett. **70**, 3111 (1993).
[11] H.E. Brauer, H.I. Starnberg, L.J. Holleboom, V.N. Strocov, and H.P. Hughes, Phys. Rev. B **58**, 10 031 (1998).
[12] V.N. Strocov, H.I. Starnberg, P.O. Nilsson, H.E. Brauer, and L.J. Holleboom, Phys. Rev. Lett. **79**, 467 (1997).
[13] C. Wang, C.G. Slough, and R.V. Coleman, J. Vac. Sci. Technol. B **9**, 1048 (1991).
[14] I. Ekvall, H.E. Brauer, E. Wahlström, and H. Olin, Phys. Rev. B **59**, 7751 (1999).
[15] S.C. Bayliss and W.Y. Liang, J. Phys. C **17**, 2193 (1984).
[16] G.V. Kamarchuk, A.V. Khotkevich, V.M. Bagatsky, V.G. Ivanov, P. Molinié, A. Leblanc, and E. Faulques, Phys. Rev. B **63**, 073107 (2001).
[17] K. Hayashi and M. Nakahira, J. Solid State Chem. **24**, 153 (1978).
[18] Th. Pillo, J. Hayoz, H. Berger, M. Grioni, L. Schlapbach, and P. Aebi, Phys. Rev. Lett. **83**, 3494 (1999).
[19] Th. Pillo, J. Hayoz, H. Berger, R. Fasel, L. Schlapbach, and P. Aebi, Phys. Rev. B **62**, 4277 (2000).
[20] K. Horiba, K. Ono, J.H. Oh, T. Kihara, S. Nakazono, M. Oshima, O. Shiino, H.W. Yeom, A. Kakizaki, and Y. Aiura, Phys. Rev. B **66**, 073106 (2002).
[21] L. Perfetti, A. Georges, S. Florens, S. Biermann, S. Mitrovic, H. Berger, Y. Tomm, H. Höchst, and M. Grioni, Phys. Rev. Lett. **90**, 166401 (2003).
[22] F.J. Himpsel, Adv. Phys. **32**, 1 (1983).
[23] A. Zunger and A.J. Freeman, Phys. Rev. B **19**, 6001 (1979).
[24] M. Bayard and M. Sienko, Solid State Chem. **20**, 251 (1976).
[25] A. Toriumi and S. Tanaka, Physica B **105**, 141 (1981).
[26] R. Claessen, B. Burandt, H. Carstensen, and M. Skibowski, Phys. Rev. B **41**, 8270 (1990).